1   Supplementary figures for Section 5.3

In Section 5.3 of the paper we show the results in a compressive sensing recovery experiment with synthetic data for RWBP and RW_5BP. We show here two additional results. First, we show in Figure 1 the compressive sensing recovery results using Basis Pursuit (BP) as the recovery algorithm. Second, we show in Figure 2 the compressive sensing recovery results using the algorithm with divisive normalization update with neighborhood size 5 (RW_5BP). The results for BP are similar to RWBP, whereas the results for RW_5BP are similar to the results for RW_3BP.
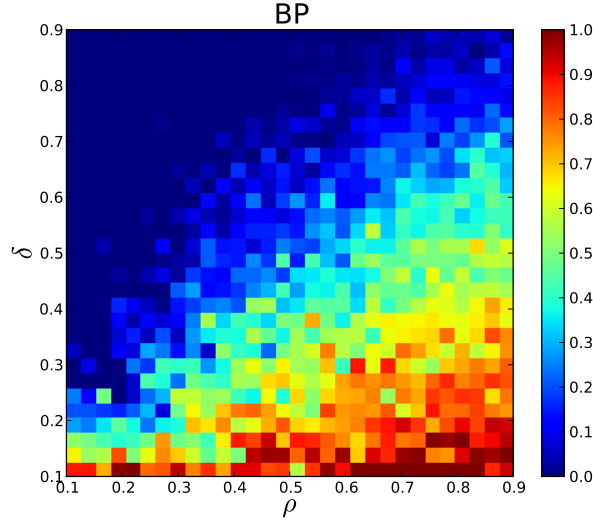

Figure 1: Compressive sensing recovery results using synthetic data. We show the phase plots for BP. On the x-axis is the sparsity of the system indexed by $\rho = 3d/m$, and on the y-axis is the indeterminacy of the system indexed by $\delta = n/m$. At each point (ρ, δ) in the phase plot, we sample 10 compressive sensing problems and display the average recovery error.

2   Supplementary figures for Section 5.4

In Section 5.4 of the paper, we describe a compressive sensing experiment applied to image patches. In the paper we have compared the recovery performance of the inference algorithm corresponding to inference in a non-factorial LSM model with 3×3 overlapping group ($RW_{3 \times 3}BP$) with the inference algorithm corresponding to inference in a factorial LSM model (RWBP). We show here how these two algorithms compare to the algorithm corresponding to inference in a factorial model with Laplacian prior (BP). We show in Figure 3 the comparison between BP and $RW_{3 \times 3}BP$, and see that $RW_{3 \times 3}BP$ clearly outperforms BP. We show in Figure 4 the comparison between BP and RWBP, and see that RWBP outperforms BP as RWBP is able to find solutions with greater sparsity.
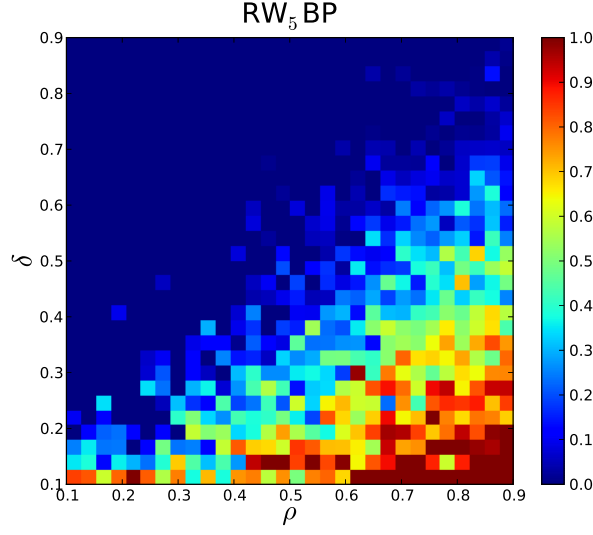
Figure 2: Compressive sensing recovery results using synthetic data. We show the phase plots for RW$_5$B. On the x-axis is the sparsity of the system indexed by $\rho = 3d/m$, and on the y-axis is the indeterminacy of the system indexed by $\delta = n/m$. At each point (ρ, δ) in the phase plot, we sample 10 compressive sensing problems and display the average recovery error.
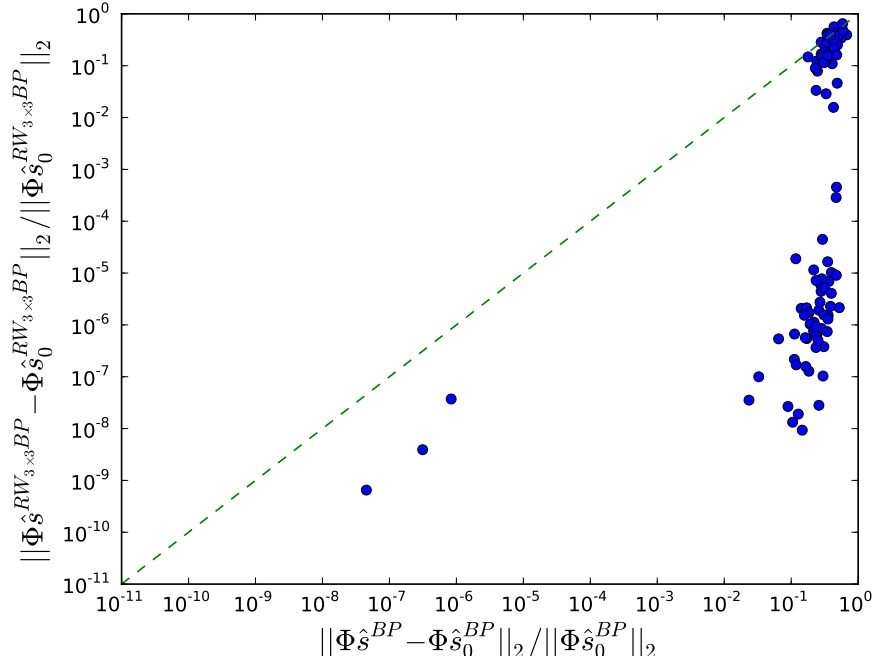

Figure 3: Compressive sensing recovery. On the x-axis is the recovery performance for the factorial Laplacian model (BP), and on the y-axis the recovery performance for the non-factorial LSM model with 3×3 overlapping groups (RW$_{3 \times 3}$BP).
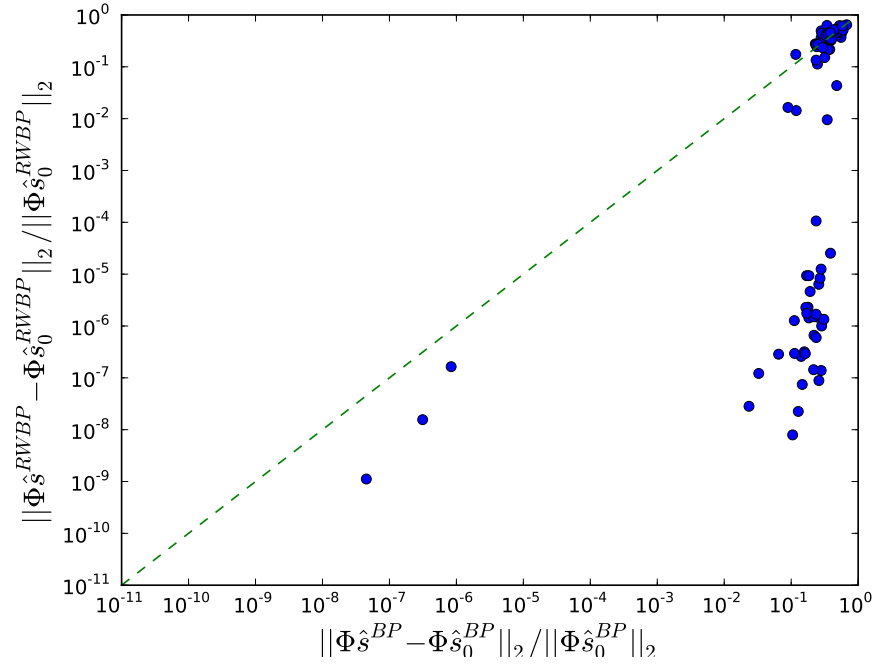
Figure 4: Compressive sensing recovery. On the x-axis is the recovery performance for the factorial Laplacian model (BP), and on the y-axis the recovery performance for the non-factorial LSM model with 3×3 overlapping groups (RW$_{3\times3}$BP).